



Midori Yano · Takayuki Itoh · Yuusuke Tanaka · Daisuke Matsuoka · Fumiaki Araki

A comparative visualization tool for ocean data analysis based on mode water regions

Received: 18 September 2019 / Revised: 12 January 2020 / Accepted: 21 January 2020 / Published online: 20 February 2020
© The Visualization Society of Japan 2020

Abstract Ocean data have been improved with the enhancement of observed values and the evolution of computational technologies. It has also been verified based on the reproducibility of various ocean phenomena. Mode water is one of the indicators for assessing ocean data because of its special properties. However, its definition differs for each ocean data. Besides, its observation is primarily performed by 2D analysis using the cutting plane of the ocean space. Therefore, reproducibility of the ocean space may have not been fully examined. Here, this paper presents a visual analysis tool for the feature of ocean data based on the 3D shape comparison of the mode water regions among three ocean datasets. Our comparison is based on similarity measure from shape appearances of the mode water regions extracted as isosurfaces. Users can interact with shape similarity data and a pair of isosurfaces. Our visualization tool supports to easily explore the relationship of different variable thresholds that are used for conditions of the mode water region and observe the specified parts of the pair in the 3D space. We demonstrate the availability and potential benefit of this approach through three examples that searched for the best conditions and expert feedback.

Keywords Comparative visualization · Scientific visualization · Volume dataset · Isosurface · Ocean data · Mode water

1 Introduction

Mode water is a type of seawater mass defined by particular water properties and distributed in the world ocean (Fig. 1). Its formation process is closely related to the condition change of air on the seawater surface. For example, subtropical mode water, one of the mode waters in the North Pacific Ocean, is formed under mainly the influence of Kuroshio and westerlies. Studies of mode water lead to understanding the mechanism of global phenomena, such as seawater flows and climate change.

Mode water forms a 3D region characterized by similar water properties. Its property is one of the criteria for evaluation of ocean data. Researchers in the field of physical oceanography have often compared the ocean data by drawing iso-contours on the cutting plane of the ocean including mode water regions

M. Yano (✉) · T. Itoh
Ochanomizu University, 2-1-1 Otsuka, Bunkyo-ku, Tokyo 112-8610, Japan
E-mail: drsn@itolab.is.ocha.ac.jp

T. Itoh
E-mail: itot@is.ocha.ac.jp

Y. Tanaka · D. Matsuoka · F. Araki
Japan Agency for Marine-Earth Science and Technology, 3173-25, Showa-machi, Kanazawa-ku, Yokohama, Kanagawa 236-0001, Japan

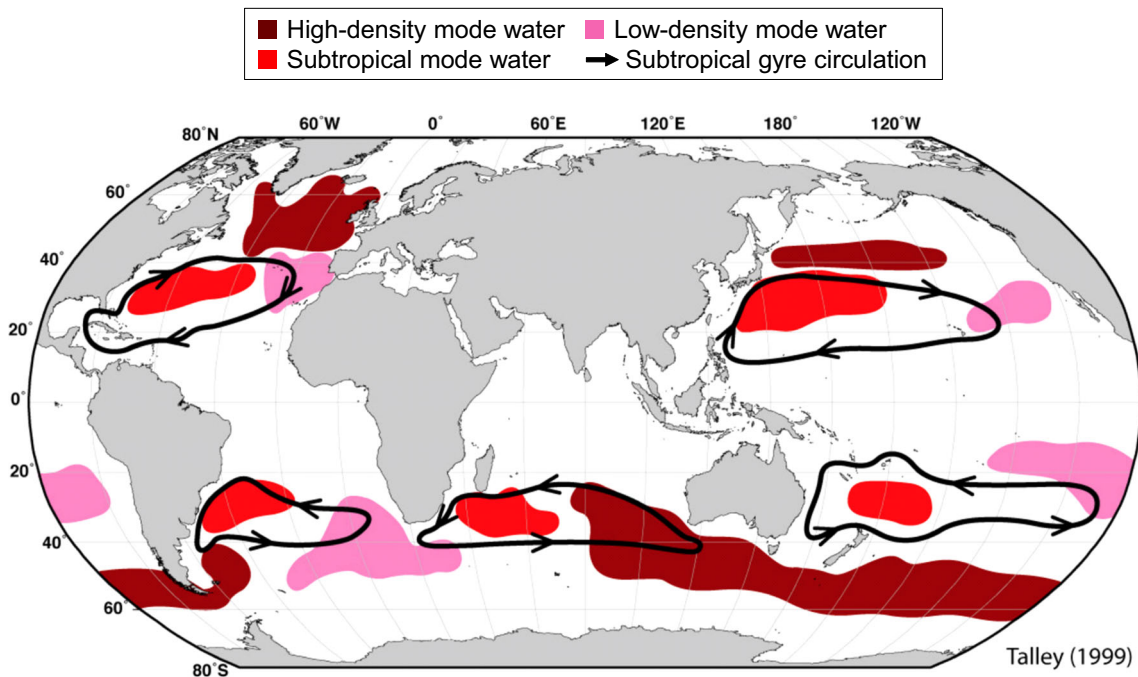


Fig. 1 Distribution of mode water in the world (Talley 1999). Each color shows a type of mode water

(Yasuda and Kitamura 2003; Usui et al. 2017). This comparison is useful to observe partial structures of mode water; however, it is not easy to reproduce the 3D structure of the ocean by observing the iso-contours. 3D shape comparison of mode water regions is important because it can contribute to the high reproduction of the 3D ocean space. Finding similar/dissimilar parts of the mode water region would be helpful to improve the understanding of ocean features in the data. An example scenario is to compare observation and simulation datasets based on the shapes of the mode water region. Dissimilar parts of shape can provide a hint of better ocean simulation.

A mode water region can be defined as a set of subregions where satisfy pre-defined conditions of physical characteristics such as temperature, salinity, and density. Several studies of mode water have been performed based on their definitions applying different sets of physical characteristics (Douglass et al. 2012; Gao et al. 2016; Masuzawa 1969; Oka et al. 2015; Yasuda and Kitamura 2003). Also, various thresholds of the physical characteristics have been applied to extract mode water regions (Davis et al. 2011; Nishikawa et al. 2010; Xu et al. 2014) appropriately. It is therefore important to analyze how different definitions of thresholds have impacts on each shape of mode water regions (Yano et al. 2018). Comparative analysis of mode water regions based on the different definitions of thresholds would be effective to comprehend 3D distributions of physical characteristics in the ocean.

In this paper, we present a 3D visualization tool for shape comparison of mode water regions applying the different conditions to evaluate ocean data. We suppose to compare two volume datasets generated by each ocean dataset of the same ocean region. We generate isosurfaces as outer boundaries of mode water regions from each ocean dataset and calculate the similarity between the isosurfaces by a view-based method, one of the 3D shape comparison methods. Isosurfaces are generated based on the different conditions from each ocean dataset. The visualization tool displays the set of similarity values as multi-dimensional time series data. We can observe the tendency of similarity values based on the conditions of mode water regions of each ocean dataset. Moreover, we can select a pair of mode water regions based on a condition and observe the pair of their isosurfaces.

This paper is an extended version of our conference paper (Yano et al. 2018): the paper introduces the comparative experiments applying three ocean datasets (observation (Locarnini et al. 2013; Zweng et al. 2013), simulation (Masumoto et al. 2004), and assimilation (Usui et al. 2017)) based on the mode water regions.

Table 1 References which define mode water

References	Data	PV	Density
Xu et al. (2014)	ARGO	$< 1.5 \times 10^{-10}$	24.9–25.5
Xu et al. (2014)	OFES	$< 1.5 \times 10^{-10}$	25.2–25.6
Xu et al. (2014)	POPH	$< 1.5 \times 10^{-10}$	24.8–25.3
Xu et al. (2014)	POPL	$< 1.5 \times 10^{-10}$	25.3–25.8
Davis et al. (2011)	ECCO2	$< 2.0 \times 10^{-10}$	25.0–25.6
Nishikawa et al. (2010)	OGCM	$< 2.0 \times 10^{-10}$	24.8–25.3

Our contributions are:

- Comparison of the mode water regions by implementing a view-based 3D shape comparison method (Sect. 3.2).
- Visualization of shape similarity data and a pair of isosurfaces of the mode water regions supported by the presented tool (Sects. 3.3–3.5).
- Analysis of reproducibility of three ocean datasets based on shape comparison results of the mode water regions (Sect. 4).

The rest of this paper is organized as follows: Sect. 2 introduces the related work. In Sect. 3, we present a shape comparison procedure of the mode water regions. Section 4 describes the used ocean datasets, the conditions to extract mode water regions and the shape comparison results of the mode water regions using our tool. Section 5 provides expert feedback on the tool and results. We discuss the advantages and limitations of the tool and future work in Sect. 6 and conclude in Sect. 7.

2 Related work

This section explains the definition and role of mode water, isosurface-based comparison visualization, and 3D shape comparison.

2.1 Definition of mode water

Mode water has been defined with physical characteristics by different variables (Douglass et al. 2012; Gao et al. 2016; Masuzawa 1969; Oka et al. 2015; Yasuda and Kitamura 2003). For example, (Masuzawa 1969) defined the North Pacific subtropical mode water with temperature and salinity. Yasuda et al. (Yasuda and Kitamura 2003) defined it with temperature and gradient of temperature.

A mode water region is defined as a closed 3D region of the ocean where physical characteristics of the seawater satisfy a pre-defined set of conditions. Table 1 shows examples of variable thresholds corresponding to the conditions of the same mode water as above. Here, the term “PV” stands for potential vorticity and is a vertical gradient of “density.” The term “density” is a value calculated from temperature, pressure, and salinity (Tenth 1981). This table suggests there are various definitions of variable thresholds among the used ocean data. We have implied that different definitions of thresholds affect shapes of the same mode water in the previous work (Yano et al. 2018). In this work, we compare three types of ocean data based on shape comparison of the same mode water regions with different thresholds. We expect that shape comparison results would be effective to comprehend 3D distributions of physical characteristics and assist the process of reproduction for each ocean data.

2.2 Comparison of ocean data based on mode water

Mode water is applied as one of the criteria for the comparison of ocean data. It has been used to visualize by drawing iso-contours on the cutting plane of the ocean to compare ocean data (Yasuda and Kitamura 2003; Usui et al. 2017). Usui et al. (2017) showed differences in temperature between compared datasets in addition to the above observation. It is possible to analyze the reproduction in the specific position of the ocean; however, researchers cannot easily recognize differences in 3D distributions between the compared datasets. Meanwhile, 3D analysis of the ocean phenomena gets more important recently. For example, ocean eddies are applied to isosurface visualization to observe their variation (Liu et al. 2017). Research on the main pycnostad water of subtropical mode water in the North Pacific Ocean required 3D structure analysis

for further study (Toyama and Suga 2011). This paper presents our 3D shape comparison of mode water regions among ocean datasets and analysis of the spatial differences between the ocean datasets aiming the better reproduction. We expect 3D visualization techniques would help mode water analysis which previously applied 2D visualization techniques.

2.3 Isosurface-based comparative visualization

Many effective techniques for isosurface-based comparative visualization have been developed. Isosurface similarity maps (Bruckner and Möller 2010; Tao et al. 2018) provided representative isosurfaces. Hazarika et al. (2018) selected the most informative isosurfaces using an information-theoretic method. These studies focused on suggesting important isovalues and understanding their corresponding isosurfaces. Alabi et al. (2012) proposed Ensemble Surface Slicing (ESS) as an ensemble data visualization technique applying sliced isosurfaces. Demir et al. (2016) visualized an ensemble of isosurfaces by a set of screen space silhouettes. Biswas et al. (2013) introduced isosurfaces applying the color-mapping representing the degree of uncertainty of variables. Hazarika et al. (2016) visualized ensemble isosurfaces applying the color-mapping representing distances from the median surface.

Our technique calculates colors of isosurfaces from distances between the arbitrary point of an isosurface and the other isosurface, as Hazarika's technique. Ocean dataset is a volume dataset that contains scalar values s_1 to s_N at each grid-point, where N is the number of scalar values. We apply the marching cubes algorithm to ocean datasets in order to extract the outer contour boundary of the mode water. It is described as the 3D region surrounding a set of grid-points which satisfy $s_{i0} < s_1 < s_{i1}$ to $s_{N0} < s_N < s_{N1}$, where s_{i0} and s_{i1} are lower and upper thresholds of the i th scalar value. Also, such regions can be perfectly reproduced as the logical product of interval volumes (Fujishiro et al. 1996).

2.4 3D shape comparison

Based on a survey conducted by ElNaghy et al. (2013), 3D shape descriptors are divided into five types; (1) view-based, (2) graph-based, (3) geometry-based, (4) statistics-based, and (5) general. View-based methods examine the similarity of appearances from images of 3D objects projected on the 2D spaces. Graph-based methods apply graph matching of 3D objects. Geometry-based methods capture geometric features directly, while statistics-based methods treat those features converted into static values. General methods are based on feedback and a combination of 3D object retrieval techniques.

Overall, view-based techniques are more discriminative than any other methods despite discarding 3D information of an object as discussed in (Chen et al. 2003; Shilane et al. 2004; Bimbo and Pala 2006). This is because geometry-based comparison tends to deal with high-dimensional values to capture salient features. Statistics-based comparison tends to lack accuracy because the spatial distribution of object features is not taken into account. On the other hand, the process of view-based comparison, such as image acquisition and feature extraction, is not complicated. Therefore, we apply a view-based shape comparison technique in this work. Actually, the view-based method is widely applied to 3D shape recognition (Su et al. 2015; Qi et al. 2016).

Our implementation of view-based methods places a target shape at the center of a polyhedron. Vertices of the polyhedron are treated as viewpoints so that we can arrange viewpoints uniformly. An octahedron (6 viewpoints) (Vranic and Saupe 2004), a dodecahedron (20 viewpoints) (Chen et al. 2003), and an icosahedron (42 viewpoints) (Ohbuchi et al. 2008) have been applied as typical polyhedrons. Here, it is not easy to estimate the optimal number of viewpoints because we have multiple factors including accuracy and computational complexity. Lian et al. (2010) presented that the use of a large number of viewpoints does not always perform well. According to several discussions on the number of viewpoints, comparison results using 20 viewpoints are better than those using six viewpoints (Chaouch and Verroust-Blondet 2007). On the other hand, except in the case of comparison of articulated shapes, no significant differences are observed between comparison results using 20 and 42 viewpoints (Ohbuchi et al. 2008).

In addition to the above studies, (Chen et al. 2003) proposed that the 20 viewpoints could roughly represent a 3D object based on previous studies (Lindstrom and Turk 2000; Huber and Hebert 2003). They put cameras on 20 vertices of a dodecahedron to collect images of a 3D object and provided better comparison results based on visual similarity than those using any other methods. Several view-based techniques are using images from vertices of a dodecahedron (Lin et al. 2018; Shih and Chen 2006) similar to Chen's work. Recently, images of a 3D object rendering from vertices of a dodecahedron have been applied to shape comparison combining deep learning (Xie et al. 2015; Han et al. 2017).

We measured the computation time for acquisitions of a series of 20 images on our running environment with Java Development Kit (JDK) 1.8.0 and found that at least 350 ms is required after every frame acquisition. It takes about 8.1 min to calculate feature vectors of 20 shapes generated from a one-month dataset and 13.12 ms to calculate the shape similarity value of a pair. Therefore, we take about 25.6 h to compare all shapes in this study, including about 21 h to calculate feature vectors of all shapes and 4.6 h to calculate the similarity of all pairs. We will require about twice the computation time as long as the above-mentioned if we take the number of viewpoints as 42. Based on these discussions and experiments, we experimentally place the shape of the mode water region into a dodecahedron.

One disadvantage of the view-based method using silhouette images is to overlook dents or cavities of a target 3D object. As referred to Sect. 2.2, there have been observations of the rough outline of mode water regions and discussions on the relationship of ocean phenomena; however, these studies did not focus on the detail of shapes of mode water regions. Besides, the cutting plane including a center part of the mode water region shows that large dents or cavities are not formed based on the distribution of PV and density from observation datasets (Xu et al. 2017). In physical oceanography, there are weak diffusions caused by ocean currents to keep isodensity under the ocean. For that reason, the dent parts are hardly formed in a center part of mode water regions. Even if there are dent parts, the parts have been not emphasized in previous works of mode water regions. Therefore, the above-mentioned disadvantage is not an important problem in our work.

3 Design of the presented tool

We describe the processing flow of shape comparison of the mode water regions in this section, as illustrated in Fig. 2. We first extract outer boundaries of the mode water regions as isosurfaces from each volume dataset, where scalar values are assigned to each grid-point. We then perform 3D shape comparison of mode water regions by a view-based method and calculate their shape similarity. We visualize the similarity values and a pair of isosurfaces using the tool.

We select a type of datasets and set conditions of the mode water region while generating isosurfaces. In this study, we suppose that multiple isosurfaces can be extracted from a single volume dataset by repeating the isosurface generation while adjusting the conditions of the mode water region. We also suppose that isosurfaces can be extracted at multiple time steps if the dataset is a time-varying volume. As a result, we can compare one-to-multiple isosurfaces and treat their similarity values as multi-dimensional time series data. Our tool visualizes the multi-dimensional time series data in a time series plot and user-selected pairs

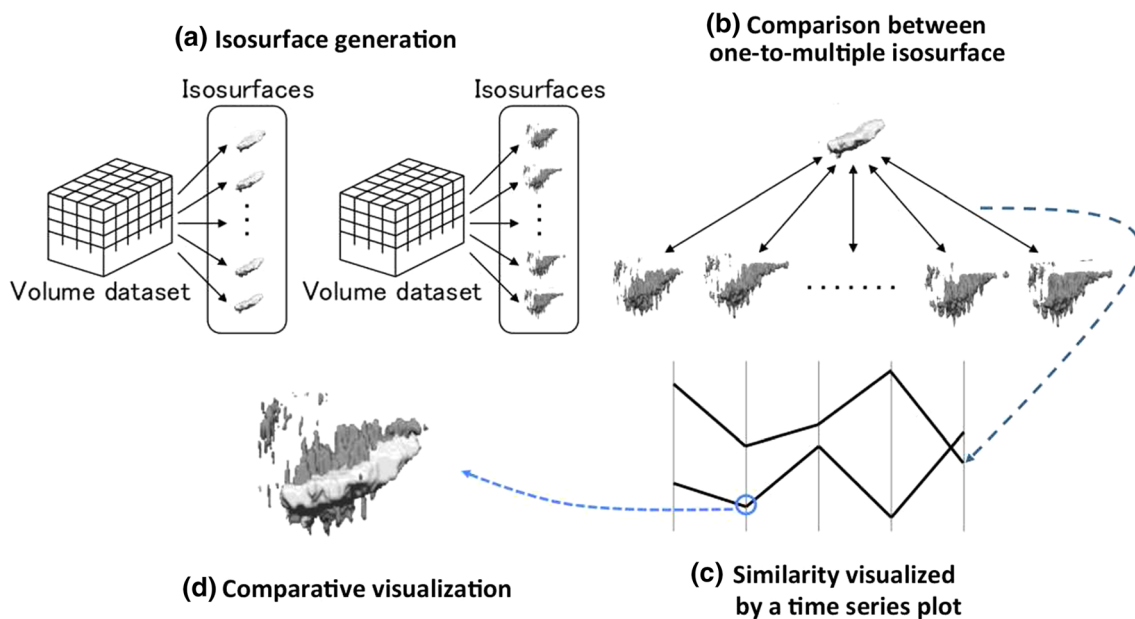


Fig. 2 Processing flow; **a** multiple isosurfaces generation from a single volume dataset, **b** comparison between one-to-multiple isosurfaces, **c** similarity data visualization and **d** comparative visualization in the tool

of isosurfaces. Here, since this visualization gives an overview of a series of shape similarity values, users can observe easily the specified pairs of isosurfaces with a shape similarity value by click operations.

3.1 3D outer boundary extraction

We generate isosurfaces by extracting the 3D outer boundary of mode water regions using the tool. We first generate an additional scalar field in each volume dataset. A positive value is assigned to a grid-point if it satisfies all the condition. Otherwise, a negative value is assigned. We then extract an isosurface from a set of points satisfying that the scalar value is zero and treat the outer surfaces as the 3D outer boundary of a mode water region in this study.

3.2 3D shape comparison

We calculate the shape similarity to compare pairs of isosurfaces. We implement a view-based shape comparison method that generates a polyhedron surrounding a target object and treats vertices of the polyhedron as viewpoints (Fig. 3). In this implementation, we generate a dodecahedron and place an isosurface of mode water region inside the dodecahedron. We can obtain 20 images of the isosurface from different viewpoints that are vertices of the dodecahedron. Then, we extract the outer contour of the isosurface from each image and convert pixels P_k to the polar coordinates (r_k, θ_k) . We generate a 2D histogram (r, θ) that is normalized with the mean distance of r and regard frequency as a feature vector. Let $X_p = \{p_1, p_2, \dots, p_{20}\}$ be a set of feature vectors at each viewpoint of shape X , where p_i is a feature vector generated with the i th viewpoint. Also, let $Y_q = \{q_1, q_2, \dots, q_{20}\}$ be a set of feature vectors at each viewpoint of shape Y , where q_j is a feature vector generated with the j th viewpoint. We calculate the Manhattan distance between X_p and Y_q at each viewpoint by $d(p_i, q_i) = |p_i - q_i|$. Then, we calculate the mean distance $D(X, Y) = \frac{1}{20} \sum_{i=1}^{20} d(p_i, q_i)$ and treat it dissimilarity between shape X and shape Y .

3.3 Visualization for similarity data

We generate multiple isosurfaces from each volume dataset applying different conditions of the mode water region. Therefore, we calculate multiple similarity values between an isosurface generated from one of the volume datasets and multiple isosurfaces generated from another volume dataset. In this study, we compare isosurfaces generated from an observation dataset with those generated from the other datasets. We visualize the similarity values as multi-dimensional time series data in a time series plot of the tool. The number of axes corresponds to years of the other datasets compared with the observation dataset. The range of axes corresponds to the range of similarity values. Smaller dissimilarity is depicted on the lower side of the axis. One polyline shows a time series of dissimilarity of a pair of isosurfaces generated from the observation and other datasets. Colors of polylines are assigned based on the user-selected condition. Polylines of the same condition are aggregated and displayed as a band to avoid visual cluttering. Users can filter the polylines to observe the specific pairs of isosurfaces by click operations.

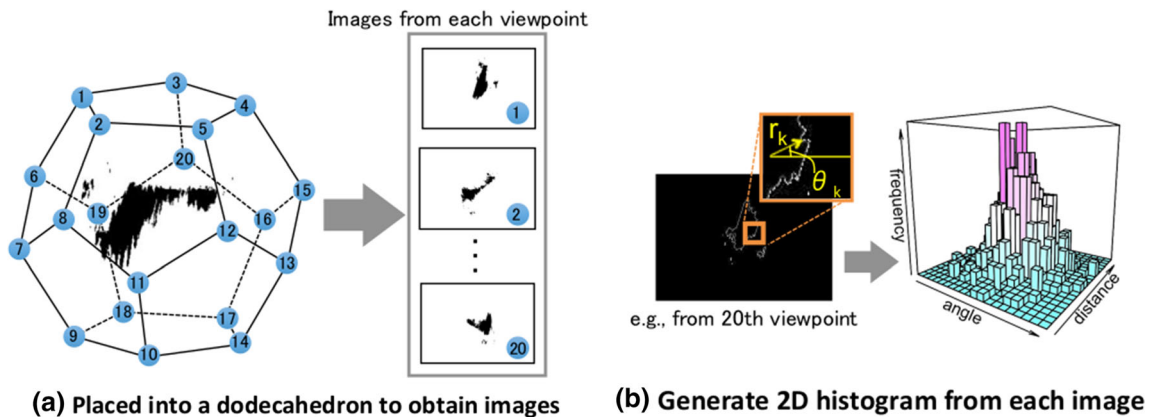


Fig. 3 View-based 3D shape comparison; **a** image acquisition and **b** feature extraction

3.4 Comparison visualization for isosurfaces

A pair of isosurfaces is displayed according to the user-selected condition in the tool. Users can observe the specified pair by clicking a particular polyline vertex in a time series plot. The color of a vertex of an isosurface is calculated based on the distance from the vertex of the other isosurface. This coloring finely represents which portions of isosurfaces are similar/different to each other. Users can interactively control the transparency of each of a pair.

3.5 User interface

We design a 3D visualization tool for shape comparison of mode water regions. Our goals are to analyze the features of each ocean data based on comparison results of the mode water region and help the high reproduction of each ocean data. This tool assists the following tasks to archive our goals:

- T1 Understand the relationship between variable thresholds applied to mode water conditions.
- T2 Explore the shape dissimilarity and pairs of isosurfaces based on the user-selected condition. For example, the similar/dissimilar, same and temporal variation-based conditions.
- T3 Observe the specified parts such as similar/dissimilar by comparing pairs of isosurfaces.

Figure 4 shows a snapshot of the user interface of the visualization tool presented in this paper. The tool provides a time series plot for a shape dissimilarity data and a specified pair of isosurfaces for shape comparison in the center of the window [Fig. 4(1)(2)]. Users can check interactively a pair of isosurfaces corresponding to a pair of vertices on the time series plot. The tool enables to visualize above tasks as follows:

- Polylines of the same condition are aggregated and displayed as a band to avoid the decline of visibility and compare the tendency of data easily (T1) in the time series plot. In addition to the color for each threshold of variables, a band is colored based on the variance value for every year of the band. A large variance shows red and a small one shows blue in the band frame.
- To observe polylines of the user-selected condition (T2), the interface widget for a polyline filtering is placed in the right of the window [Fig. 4(3)]. Besides, a pair of isosurfaces is displayed according to the user-selected condition (T2). The transparency of each isosurface can be controlled by adjusting the slider of the isosurface setting in the right of the window [Fig. 4(4)].

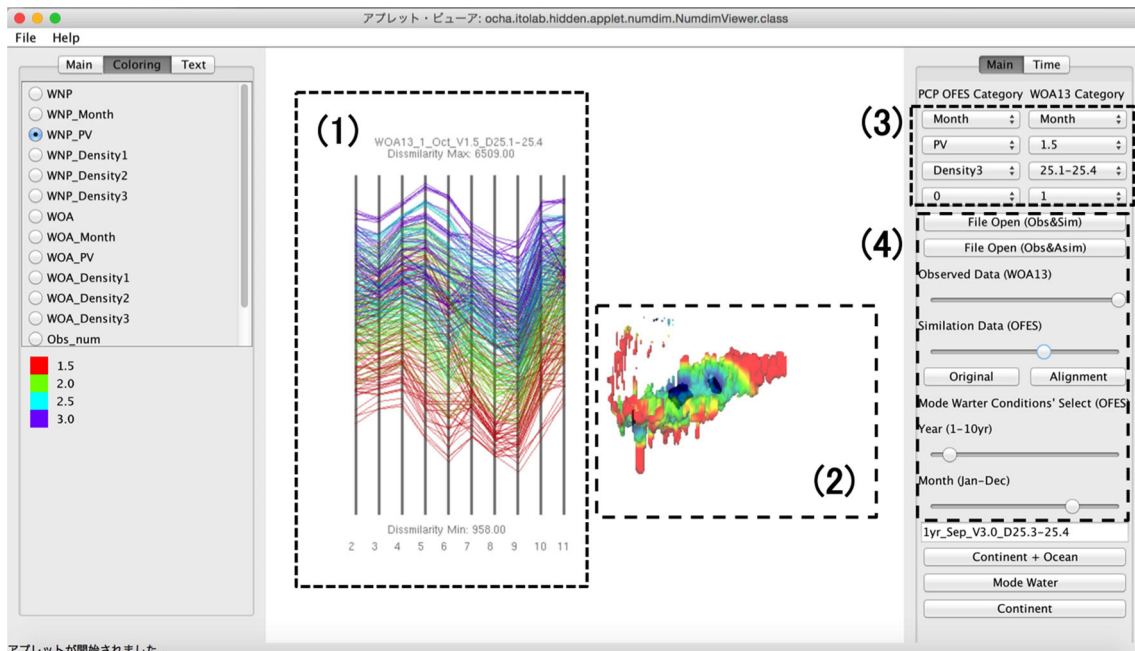


Fig. 4 User interface of the tool; (1) a time series plot for a shape dissimilarity data, (2) a pair of isosurfaces for shape comparison, (3) a polyline filtering, and (4) isosurface setting

- The color of an isosurface is calculated based on the distance from the vertex of the isosurface to the other isosurface (T3). A dissimilar part of isosurfaces is colored in red and a similar one is colored in blue.

4 Result

We experimented to compare mode water regions of three ocean datasets, observation, simulation, and assimilation. We employed an observation dataset from WOA13 (World Ocean Atlas 2013) (Locarnini et al. 2013; Zweng et al. 2013), an assimilation dataset from FORA-WNP30 (Four-dimensional variational Ocean ReAnalysis for the Western North Pacific) (Usui et al. 2017), and a simulation dataset from OFES (Ocean general circulation model simulation For Earth Simulator) (Masumoto et al. 2004).

The WOA13 and OFES datasets have a set of monthly type data, whereas the FORA-WNP30 dataset has a set of daily type data. WOA13 is a regular volume consisting of rectangular elements sized as 1.0° latitude/longitude. Meanwhile, FORA-WNP30 and OFES are also regular volumes consisting of rectangular elements sized as 1.0° latitude/longitude. We interpolated depth values at a one-meter interval in the used region, as these datasets are irregular volumes in the depth level. Grid-points of these volume datasets have PV and density values based on salinity and temperature values.

We supposed the following conditions to extract mode water regions from the WOA13, FORA-WNP30, and OFES datasets:

- *Usage month* July, August, September, or October (WOA13 only)
- *PV threshold* $PV < 1.5 \times 10^{-10}, PV < 2.0 \times 10^{-10},$
 $PV < 2.5 \times 10^{-10}, \text{ or } PV < 3.0 \times 10^{-10}$
- *Density threshold* $25.1 \leq \text{density} \leq 25.4, 25.2 \leq \text{density} \leq 25.4,$
 $25.2 \leq \text{density} \leq 25.5, 25.3 \leq \text{density} \leq 25.4, \text{ or } 25.3 \leq \text{density} \leq 25.5$

The combination of the above conditions brings 20 shapes for one-month data. We generated 480 shapes for six periods (1: 2005 to 2012, 2: 1995 to 2004, 3: 1985 to 1994, 4: 1975 to 1984, 5: 1965 to 1974 and 6: 1955 to 1964) from the WOA13 dataset, 600 shapes for 10 years from the OFES dataset and 2040 shapes for 34 years (1982–2015) from the FORA-WNP30 dataset.

4.1 Overview of comparison results among the observations, simulations, and assimilations

Figure 5 (left) shows a comparison result between the observations and the assimilations. We treated the similarity values for 34 years of the assimilation dataset as 34-dimensional time series data. It displays 4800 of 34-dimensional similarity data. Figure 5 (right) shows a comparison result between the observations and the simulations. We treated the similarity values for 10 years of the simulation dataset as 10-dimensional time series data. It displays 4800 of 10-dimensional similarity data.

As we mentioned in Sect. 3.5 that polylines of the same conditions are aggregated and displayed as a band, Fig. 5 shows bands in each comparison result are colored based on each period of the observation dataset. Here, the range of each axis is fixed to compare the two results. Compared the two results in Fig. 5, pairs of the observations and the assimilations cover smaller dissimilarity than those of the observations and the simulations. Therefore, the assimilations are more similar than the simulations to the observations. However, we did not find shapes in detail which part is similar/dissimilar between the compared shapes. In this paper, we show isosurfaces of mode water regions applied to the conditions to be a focus on after Sect. 4.2.

As referred to Sect. 3.3, the polyline of a pair that has smaller dissimilarity is focused on the lower side of each axis. We can observe a common tendency that the minimum dissimilarity for each period of the observations is obviously different between the two results. The minimum dissimilarity gets smaller as the period of the observations gets newer. The first period (colored in red) of the observations is most similar to both the assimilations and the simulations. The two results are notably different in the distribution of the sixth period (colored in magenta). Compared to the assimilations in Fig. 5 (left), the minimum dissimilarity of the sixth period is larger than those of any other periods. Also, the band of the sixth period is distributed

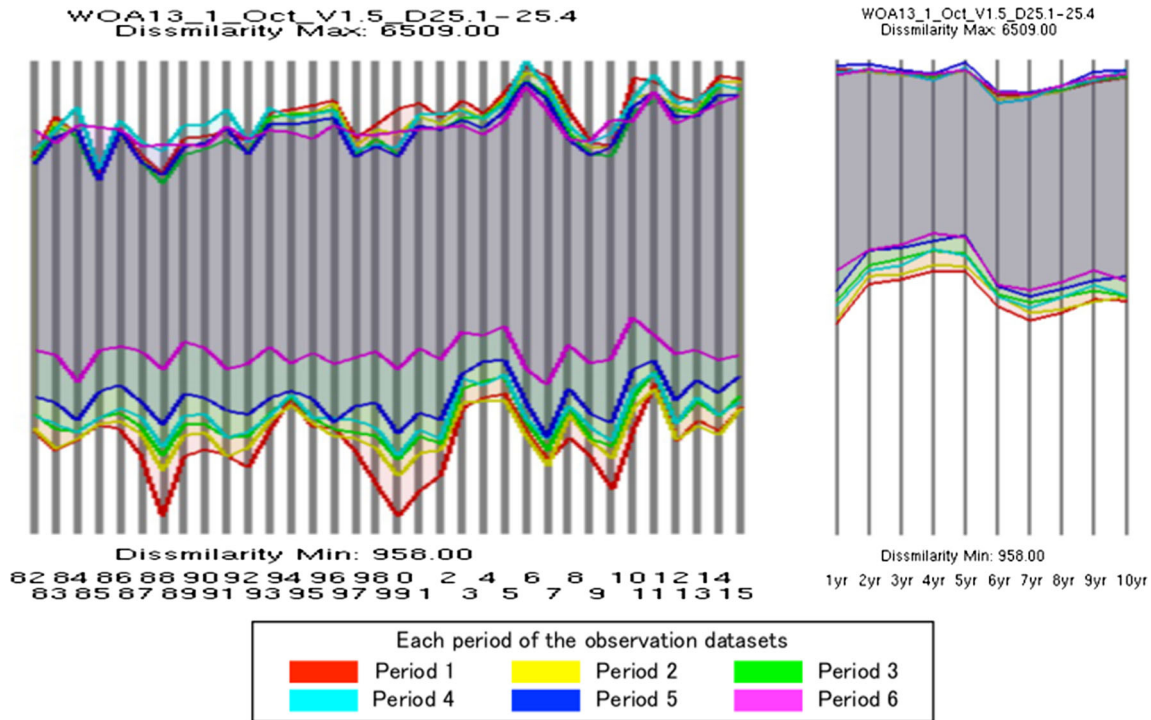


Fig. 5 (Left) A comparison result between the observations and the assimilations. (Right) A comparison result between the observations and the simulations. The range of each axis in each result is fixed. Colors of bands in each result are assigned based on each period of the observation dataset (period 1: red, 2: yellow, 3: light green, 4: cyan, 5: blue, and 6: magenta)

in a range of large dissimilarity. This is because the sixth period (1955–1964) is outermost from the period (1982–2012) of the assimilation dataset. Actually, the fourth and fifth periods (colored in cyan and blue) are over the period of the assimilation dataset, but the distributions of the two periods are not different as much as the sixth period. We suppose that the observed ocean condition of the sixth period is different from the assimilation dataset. Whereas compared to the simulations in Fig. 5 (right), the distributions between the sixth and fifth periods are not so much different. We do not know how such differences between ocean datasets are generated, but the detailed analysis of that may bring a hint for generating a better ocean dataset.

Users can observe pairs of isosurfaces of mode water regions applied to the conditions using our tool. The following sections show three examples.

4.2 Example 1: similar/dissimilar condition search

We filtered the polylines with each threshold of variables and observed their distributions. We easily found similar/dissimilar conditions between the compared pairs of mode water regions by following the distribution that is drawn with a focus on the lower/higher side of each axis. Figure 6 shows an example process of a similar condition search. We colored the bands based on thresholds of PV and found that a band colored in red ($PV < 1.5 \times 10^{-10}$) was focused on the lower of each axis in Fig. 6a. Then, we filtered the band with the above condition, colored the remaining band based on thresholds of density and finally found that a band colored in blue ($25.3 \leq \text{density} \leq 25.4$) was focused on the lower of each axis in Fig. 6b. Then, we filtered the band with the above condition and colored the remaining band based on months, as shown in Fig. 6c.

In terms of the assimilations, the condition ($PV < 1.5 \times 10^{-10}$ and $25.3 \leq \text{density} \leq 25.4$) of the assimilations was most similar to each period of the observations. In terms of the simulations, the most similar conditions to each period of the observations were the same condition as the assimilations. We found that the most similar condition to the observations was the same as both the assimilations and the simulations. On the other hand, quite different distributions were observed for each period compared with the assimilations or the simulations, in terms of the observations. We observed a tendency of each period that larger the threshold value was as larger the minimum dissimilarity was, only for PV of the observations. Also, we observed the same tendency of pairs of the observations and the assimilations regarding the

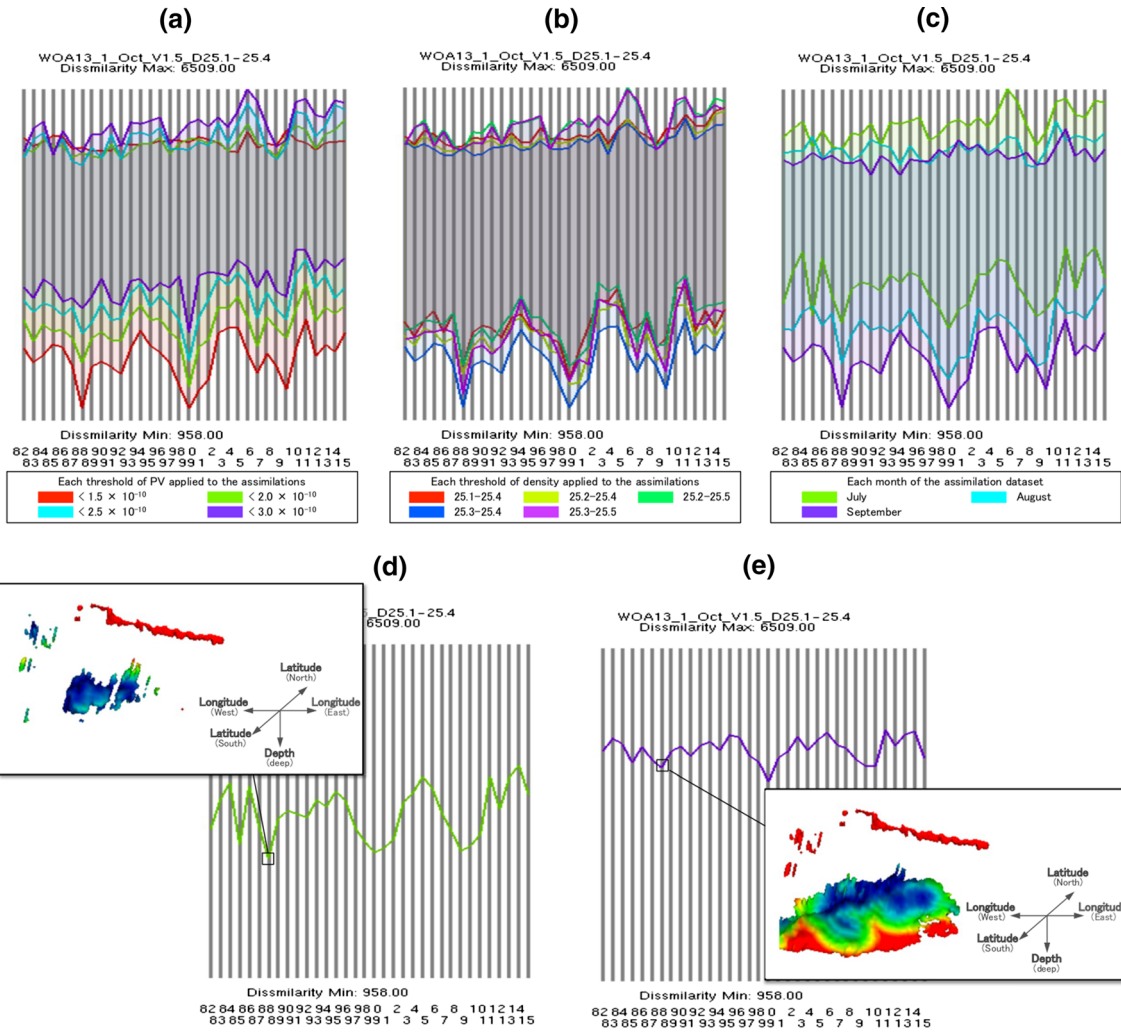


Fig. 6 An example process of a similar condition in pairs of the assimilations and the observations of the first period. **a-c** show filtered results based on variables applying the assimilations; **a** colored based on four thresholds of PV, **b** colored based on five thresholds of density, and **c** colored based on three months. We show a similar/dissimilar pair of the observation and the assimilation ($PV < 1.5 \times 10^{-10}$ and $25.3 \leq \text{density} \leq 25.4$ in July), **d** the similar pair and **e** the dissimilar pair

minimum dissimilarity for each threshold of PV. Therefore, the assimilation dataset might have high reproducibility of PV.

As an example of exploration, Fig. 6d, e shows a similar/dissimilar pairs of the observation and the assimilation ($PV < 1.5 \times 10^{-10}$ and $25.3 \leq \text{density} \leq 25.4$ in July of the first period). The condition ($PV < 1.5 \times 10^{-10}$ and $25.1 \leq \text{density} \leq 25.4$ in July 1988) of the assimilation is similar, and the condition ($PV < 3.0 \times 10^{-10}$ and $25.2 \leq \text{density} \leq 25.5$ in September) of the assimilation is dissimilar to the above condition of the observation. We can observe that the similar pair in Fig. 6d is almost colored in blue, except for portions near the ocean surface and the dissimilar pair in Fig. 6e are colored not only in blue but also in red and yellow. Both pairs include portions colored in red near the ocean surface in common, which are parts of the assimilations. In the dissimilar pair, we can observe large differences in the south direction. One reason for this may be the southward movement of the mode water caused by the recirculation gyre of the Kuroshio Extension.

Comparison of mode water regions is often difficult due to definitions with different thresholds of variables. Here, we explore and propose a similar condition for one of the criteria in observing mode water regions. As an example scenario, let us suppose that the observation and the others (assimilations and/or simulations) applying the same condition are similar. This case means that the assimilation and/or simulation dataset faithfully reproduce the observation value. Also, let us suppose that the observations and the

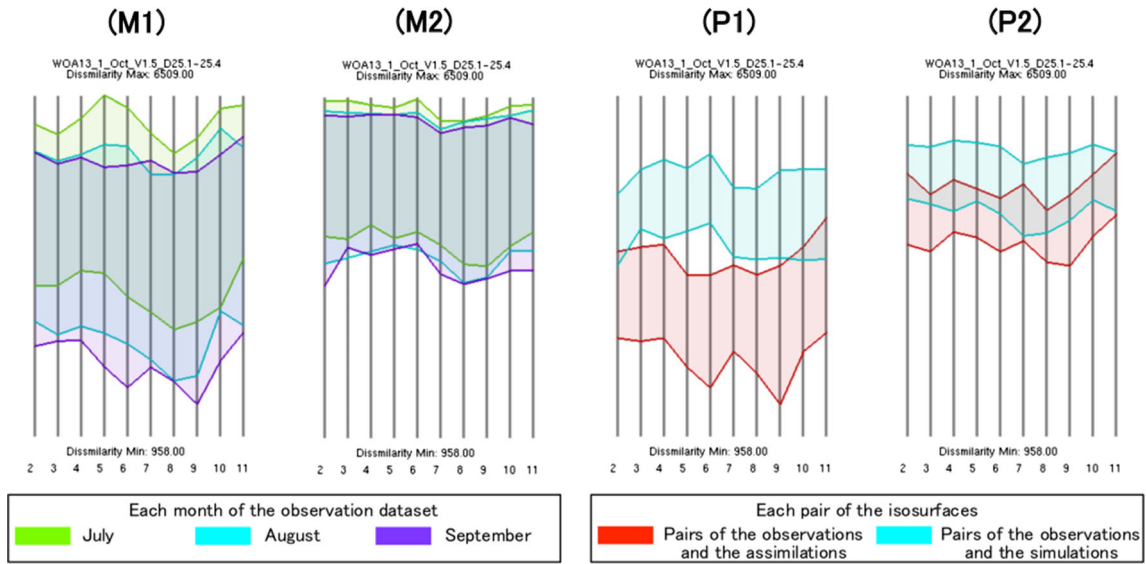


Fig. 7 Results on the left colored based on three months in (M1) pairs of the observations and the assimilations and (M2) pairs of the observations and the simulations. Results on the right colored based on the two types of pairs filtered with (P1) $PV < 1.5 \times 10^{-10}$ and (P2) $PV < 3.0 \times 10^{-10}$ in September

others (assimilations and/or simulations) applying the different condition, respectively, are similar. This case is very interesting for experts in physical oceanography because thresholds of variables are different, but those distributions are similar in 3D ocean space. The similar condition search enables the analysis of 3D distributions of variables that apply to generate isosurfaces from different ocean datasets.

4.3 Example 2: same condition search

We observed each pair of the observations and the simulations, the observations and the assimilations simultaneously. Figure 8a shows two comparison results, which a band colored in red shows pairs of the observations and the assimilations, and a band colored in cyan shows pairs of the observations and the simulations. Here, we selected the assimilations for ten years (2002–2011) corresponding to the maximum number of year of the simulations.

As mentioned in Sect. 4.1, pairs of the observations and the simulations have larger dissimilarities than those of the observations and the assimilations. We introduce the polylines filtered with the same condition in this section. For example, observing each month as shown in Fig. 7(M1) and (M2), the two types of pairs have similar distributions in July (colored in light green). On the other hand, regarding distributions in August and September (colored in cyan and purple), pairs of the observations and the assimilations cover smaller dissimilarity than those of the observations and the simulations. Also, regarding distributions of each month, pairs of the observations and the simulations keep stable with a large dissimilarity. The study in the field of physical oceanography has been reported that shapes of mode water are relatively stable in summer. Here, let us suppose that shapes generated from the observation dataset are stable. The simulations are different from the observations based on dissimilarity, but the difference is stable. Therefore, the simulation dataset reproduces the shape stability and the assimilation dataset reproduces the shape similarity except for July instead of the shape stability.

We focused on the distributions caused by different thresholds of PV. In pairs applied to the smallest threshold ($PV < 1.5 \times 10^{-10}$), pairs of the observations and the assimilations had a different distribution from those of the observations and the simulations. We observed the large differences in distributions in August and September between the two types of pairs. Whereas in pairs applied to the largest threshold ($PV < 3.0 \times 10^{-10}$), pairs of the observations and the assimilations had a similar distribution to those of the observations and the simulations. We observed distributions in July were similar between the two types of pairs, although variations of dissimilarity for each year were different. Therefore, we found that the difference in the distribution between the two types of pairs got smaller as the threshold of PV was larger. Figure 7(P1) and (P2) shows example results filtered with the smallest and largest thresholds of PV in September.

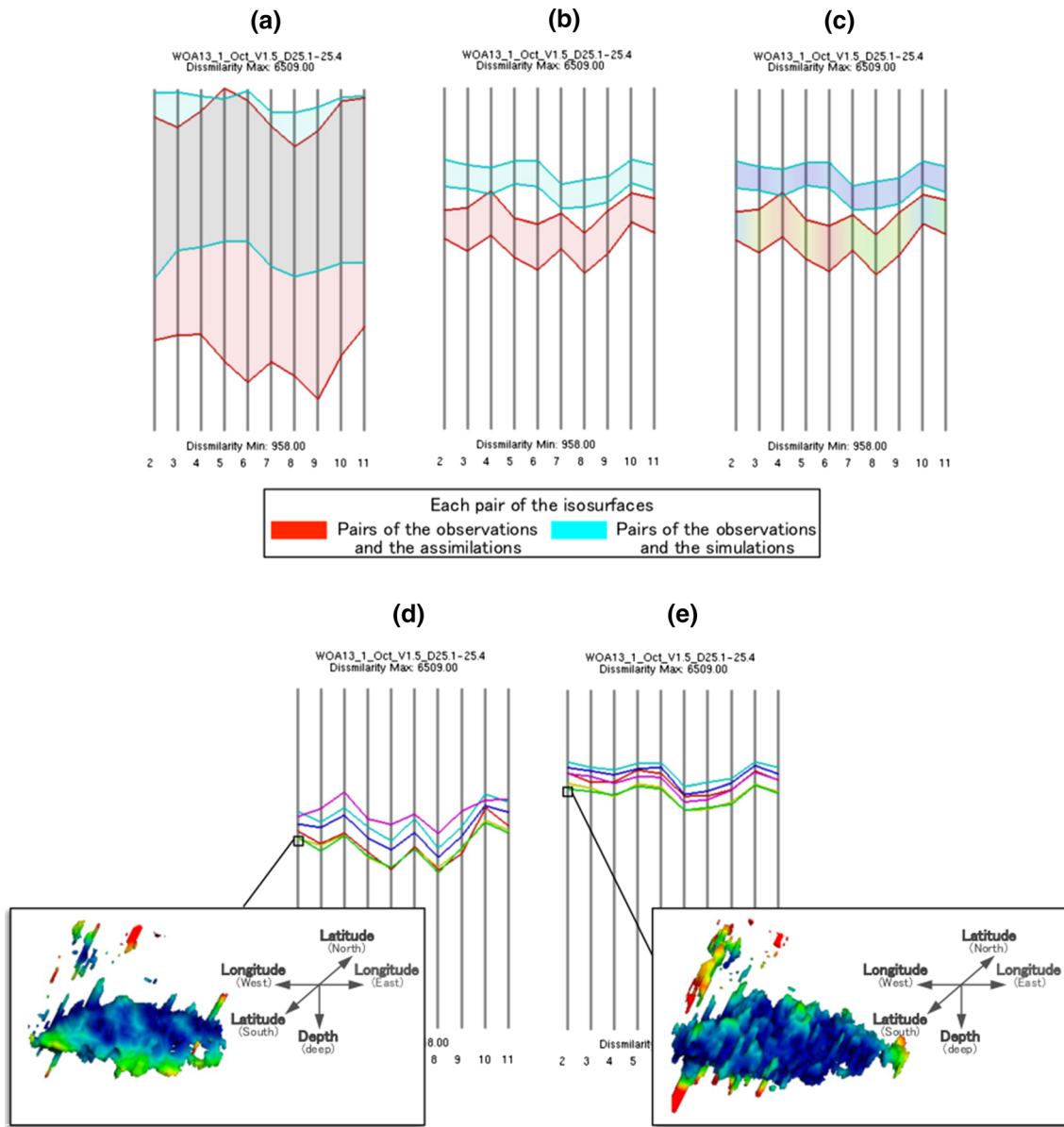


Fig. 8 An example process of the same condition in the two types of pairs; **a** overview colored based on the two types of pairs, **b** a result filtered with the same condition ($PV < 2.5 \times 10^{-10}$ and $25.1 \leq \text{density} \leq 25.4$ in September), **c** the result colored based on the variance values for every year of each band, **d** the pair of the observation of the third period and the assimilation in 2002 and **e** the pair of the observations of the third period and the simulation of the first year

This is fruitful knowledge for comparing mode water regions. In the case of the small threshold, reproducibility of observation values is different between the two types of pairs. In the case of the large threshold, reproducibility of observation values is not much different between the two types of pairs. As a result, the detailed observations of each pair of isosurfaces enable us to find similar/dissimilar parts that reproduce observation values or not. Comparison of mode water regions applied to the same condition is essential to check whether observation values are reproduced.

Figure 8 shows an example process of the same condition search. We filtered the bands with the same condition ($PV < 2.5 \times 10^{-10}$ and $25.1 \leq \text{density} \leq 25.4$ in September) as shown in Fig. 8b. Then, we colored those based on the variance values for every year of each band as shown in Fig. 8c. We observed that the band framed in cyan was colored in blue every year, but the band framed in red was colored in red, yellow, and green. We found that yearly variations of pairs of the observations and the simulations were stable. On

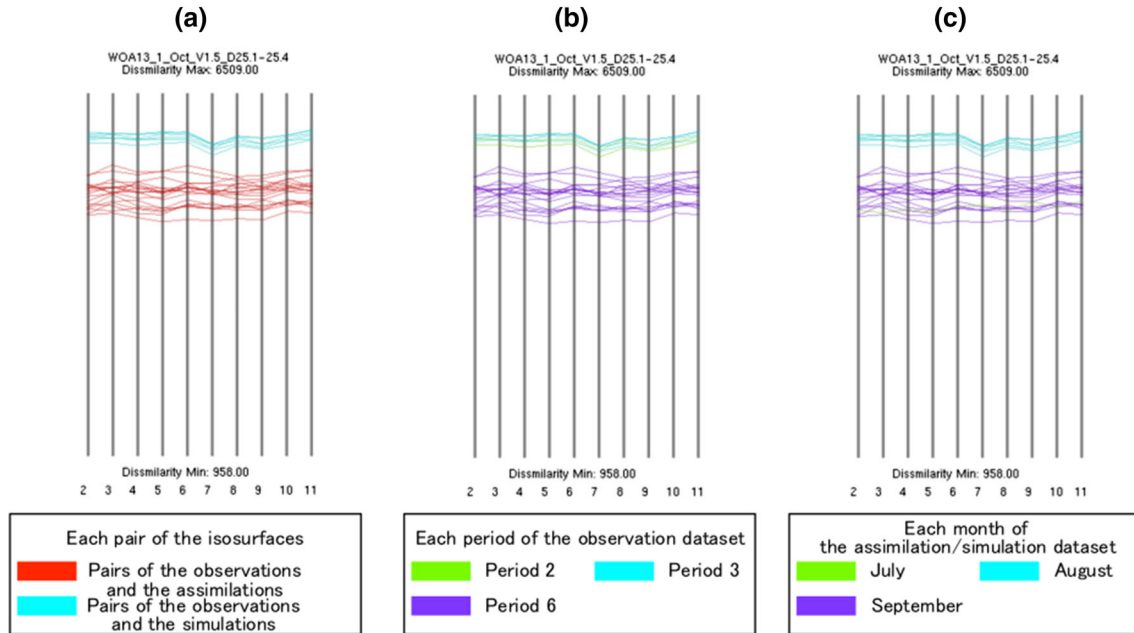


Fig. 9 Results on small temporal variations; **a** colored based on the two types of pairs, **b** colored based on six periods of the observation dataset and **c** colored based on three months of the assimilations and the simulations

the other hand, those of pairs of the observations and the assimilations were unstable; in particular, we could find the large variations in 2004 and 2006. These two years might have to be analyzed more intensively than the other eight years. Figure 8d, e shows example pairs applied to the same condition. In the pair in Fig. 8d, most parts were colored in blue except for small portions near the ocean surface. In addition, we observed small differences in the south direction. Therefore, we found that there might be small differences in reproducibility of the ocean in September between the observation and the assimilation. In the pair in Fig. 8e, most parts were colored in blue, but some portions colored in red were observed near the ocean surface and in the direction of the seabed.

4.4 Example 3: temporal variation-based condition search

We observed the polylines that temporal variation of the dissimilarity is small/large in the two types of pairs. Figure 9 shows examples that temporal variation was small for each pair. In pairs of the observations and the simulations as a band colored in cyan in Fig. 9a, we observed the polylines with the second and third periods (colored in light green and cyan in Fig. 9b) of the observations. In pairs of the observations and the assimilations as a band colored in red in Fig. 9a, we observed the polylines with the sixth period (colored in purple in Fig. 9b) of the observations. The condition of those polylines that be observed the most was as follows: the observations in October of the sixth period and the assimilations in September applying PV less than 2.0×10^{-10} .

Meanwhile, Fig. 10 shows examples that temporal variation is large for each pair. Surprisingly, there were no polylines of the pairs of the observations and the simulations. In pairs of the observations and the assimilations, the condition of those polylines that be observed the most was as follows: the observations of the first period applying $PV < 1.5 \times 10^{-10}$ and the assimilations applying $PV < 1.5 \times 10^{-10}$. Therefore, we found that many pairs of the observations and the simulations were relative smaller variations for every year than those of the observations and the assimilations. In addition, we found that there were several pairs of observations of the first period and the assimilations applying the smallest threshold of PV have large variations.

Comparison of the temporal variation is a chance to detect any variations in the ocean. The ocean is a stable state; therefore, researchers need to detect and analyze a variation in the ocean in case a state of the ocean changes. A small variation verifies that dissimilarity of the comparison pair is constant for years in our result; thus, the error from the observation value is likely to be constant. In the example pair that has small

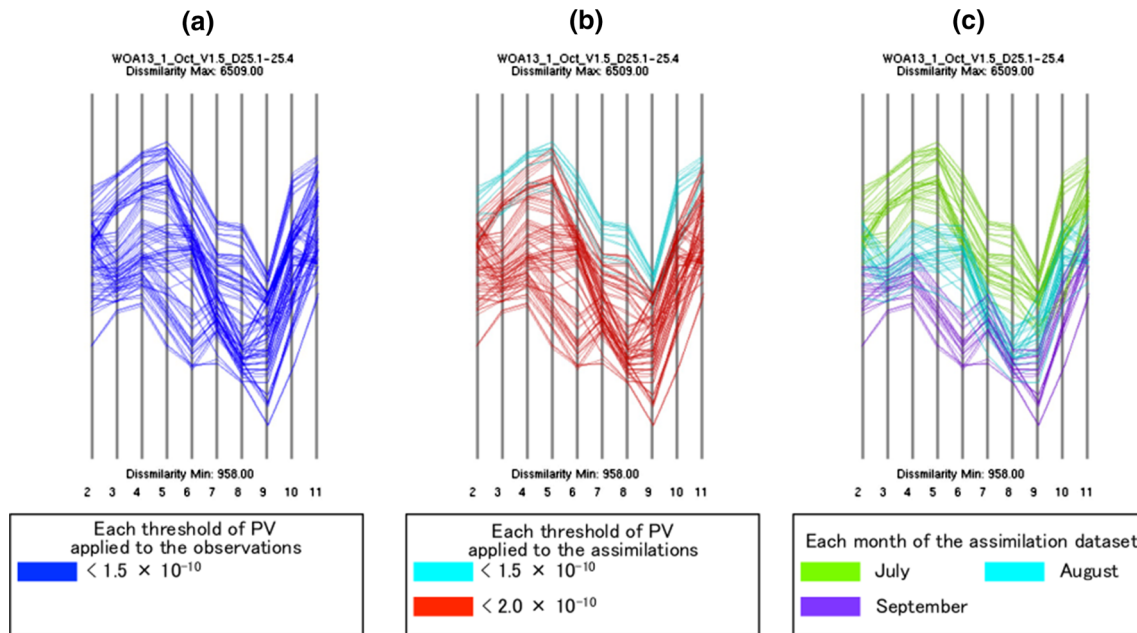


Fig. 10 Results on large temporal variations; **a** colored based on thresholds of PV applied to the observations, **b** colored based on thresholds of PV applied to the assimilations and **c** colored based on three months of the assimilations

variation, we observed that there were differences in the direction of the seabed, but almost no difference in years in Fig. 11 (Left). On the other hand, a large variation was supposed to be a case that a pair has similar and dissimilar states depending on years. For example, the band in July (colored in light green in Fig. 10c) showed that dissimilarity in 2009 was a small value and one in 2005 was a large value. We observed the pair of the above each year and found that there were differences in yearly reproducibility of the assimilations depending on the condition in Fig. 11 (right). Further analysis of these cases will be very helpful to understand the features of the ocean of each year.

We observed pairs of the observations and the simulations that the temporal variation was larger. The condition of those polylines that be observed the most was as follows: the observations in October of the fifth period applying PV more than 2.0×10^{-10} and the assimilations applying PV $< 1.5 \times 10^{-10}$. As a result, we found that several observations in October were different from those in any other month of the fifth period.

5 Expert feedback

This section introduces the feedback on the presented tool and results from an expert in physical oceanography studying the numerical models of the ocean.

The quantitative shape comparison based on dissimilarity provides a new perspective for the distribution of mode water regions. For example, the same condition search can be used as the definitive measure of the reproducibility of the ocean model. Ocean data are generated while adjusting various parameters such as temperature, salinity, wind stresses, freshwater, and heat flux that interact with each other intricately. Therefore, dissimilar parts colored in red as shown in Fig. 8d, e suggest differences in the effects of parameters, which may mean features of each ocean data.

The similar/dissimilar condition and same condition search make model improvement more efficient. Moreover, these analyses bring fundamental insights into the variation of the formation process of mode water regions. Interannual variation of atmospheric and ocean conditions may alter the density, PV, volume and shape of formed mode water regions. Therefore, the expert mentioned that this may be a powerful tool to explore the mechanism of the fluctuation of mode water regions.

The temporal variation-based condition search shows the movement of dissimilar parts, which reflect the spatial propagation of variation of the mode water region. As shown in Fig. 11 (right), the large temporal variation between 2005 and 2009 may associate with the large meander of Kuroshio occurring from 2004 to

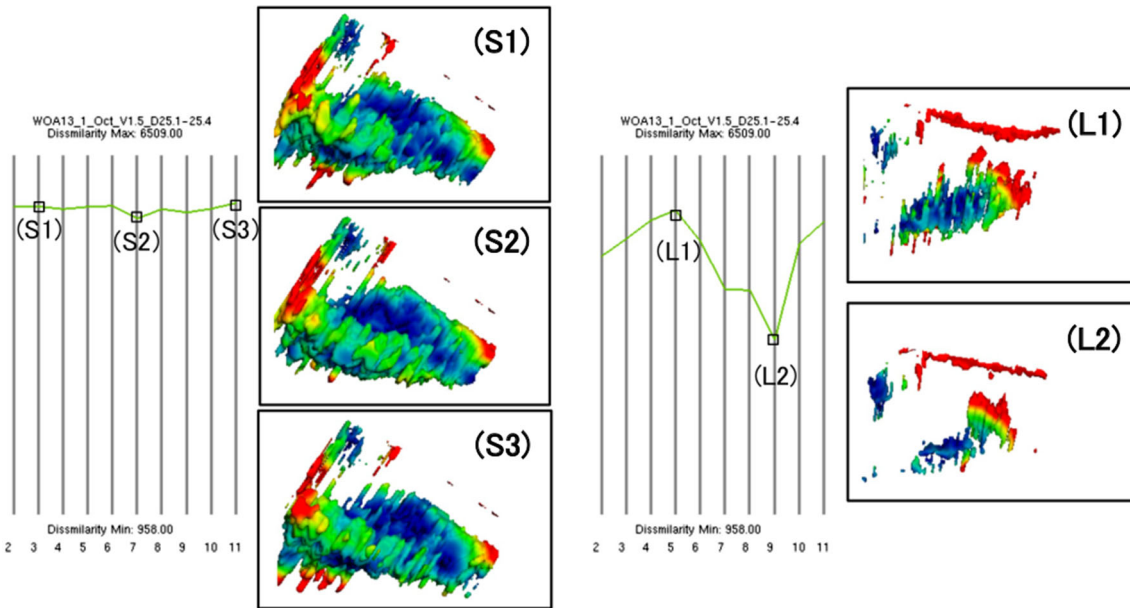


Fig. 11 (Left) Example pairs with small variation for (S1) the second year, (S2) the fourth year, and (S3) the tenth year. The condition of the pairs is as follows: the observation in July of the second period applying $PV < 2.0 \times 10^{-10}$ and $25.2 \leq \text{density} \leq 25.5$, and the simulations in August applying $PV < 3.0 \times 10^{-10}$ and $25.2 \leq \text{density} \leq 25.5$. (Right) Example pairs with large variation in (L1) 2005 and (L2) 2009. The condition of the pairs is as follows: the observation in August of the first period applying $PV < 1.5 \times 10^{-10}$ and $25.2 \leq \text{density} \leq 25.5$, and the simulations in July applying $PV < 2.0 \times 10^{-10}$ and $25.3 \leq \text{density} \leq 25.5$.

2005. As a whole, the expert mentioned that this is a promising tool for not only the validation of numerical models but also the research of mode water regions. Experts who study ocean models adjust empirically various parameters for producing ocean data. They optimize each parameter using evaluation functions (e.g., Green's function); however, the production of high-quality data is difficult because parameters interact with each other. The expert mentioned that this tool may be helpful to check the reproduction of 3D ocean space based on comparison results of mode water regions.

6 Discussion and future work

We aimed to look for the features of three ocean datasets based on shape comparison of mode water regions. The presented tool enables users to interactively explore a pair of isosurfaces based on shape similarity data. The examples of condition search described in the previous sections showed that our tool enables to observe similar/dissimilar parts of the specified pairs according to the user-selected conditions. We discovered a new tendency that cannot be identified from the differences among ocean datasets generated by observation, simulation and assimilation.

However, our tool still has remaining problems to visualize the spatial distribution of similar/dissimilar parts. Our current implementation does not provide detailed information about similar/dissimilar parts. We would like to extend the tool so that users can easily find which positions similar/dissimilar parts exist. One of our ideas is to divide the ocean space enclosing isosurfaces into voxels. We could extract a region including the specified part as a region of interest (ROI) and find local features as (Weissenböck et al. 2018). Another idea is to collect multi-fields datasets of the mode water region and examine the local distribution of physical variables that do not use for conditions of the mode water region as (Wei et al. 2017). We expect these processes would help evaluations for each ocean data based on spatial local features.

Meanwhile, we found that some shapes of the mode water region are separated into several parts. This is because some eddies satisfy the condition of the mode water region. We treat those parts as one shape of the mode water region even experts in physical oceanography have different opinions. Thereby, we observed that a pair of isosurfaces are colored in not only blue but also red even if the pair has small dissimilarity. As a further study, we would compare shapes of the mode water region taking other characteristics of mode

water such as core density into account. This comparison would help to analyze the spreading of the mode water region discussed in Nishikawa et al. (2010).

In addition to the above extensions, we will improve and apply other visualization techniques to shape similarity data in the future as follows:

- Improvement of polyline rendering in a time series plot. Bundling (Zhou et al. 2008) and highlighted function (Johansson et al. 2006) could make easier to understand the overview of shape similarity data.
- Additional filtering function. Filtering based on the user-selected polyline could promote more interactive explorations.
- Other representations for shape similarity data. We could find a new pattern from shape similarity data using MDS and t-SNE.

Our final goal in this study is to suggest the optimal parameterization for the generation of high-quality ocean data. We would assist ocean data specialized in the reproducibility of the mode water region.

7 Conclusion

We presented a 3D visualization tool for shape comparison of the mode water regions. Shapes of the mode water region are generated as isosurfaces from three ocean datasets (observation, simulation, assimilation) applying the conditions combining thresholds of two variables. We compared those shapes based on shape similarity data calculated by applying a view-based method. The presented tool visualizes shape similarity data as multi-dimensional time series data and a pair of isosurfaces according to the user-selected condition.

This tool provides users an overview of shape similarity data in a time series plot and detailed parts of the specified pair of isosurfaces interactively. We introduced three examples that searched for the best conditions and had positive feedback on the tool and results using the condition search. Performing the condition search is an effective approach of analyzing differences in ocean datasets based on shape comparison of the mode water regions by using the tool.

References

- Alabi OS, Wu X, Harter JM, Phadke M, Pinto L, Petersen H, Bass S, Keifer M, Zhong S, Healey CG, Taylor RM (2012) Comparative visualization of ensembles using ensemble surface slicing. In: Proceedings of SPIE, 8294
- Bimbo AD, Pala P (2006) Content-based retrieval of 3D models. *ACM Trans Multim Comput Commun Appl* 2(1):20–43
- Biswas A, Dutta S, Shen HW, Woodring J (2013) An information-aware framework for exploring multivariate data sets. *IEEE Trans Vis Comput Graph* 19(12):2683–2692
- Bruckner S, Möller T (2010) Isosurface similarity maps. *Comput Graph Forum* 29(3):773–782
- Chaouch M, Verroust-Blondet A (2007) A new descriptor for 2D depth image indexing and 3D model retrieval. In: 2007 IEEE international conference on image processing, vol 6, pp 373–376
- Chen DY, Tian XP, Shen YT, Ouhyoung M (2003) On visual similarity based 3D model retrieval. *Comput Graph Forum* 22(3):223–232
- Davis XJ, Rothstein LM, Dewar WK, Menemenlis D (2011) Numerical investigations of seasonal and interannual variability of North Pacific subtropical mode water and its implications for Pacific climate variability. *J Clim* 24(11):2648–2665
- Demir I, Kehrler J, Westermann R (2016) Screen-space silhouettes for visualizing ensembles of 3D isosurfaces. In: IEEE Pacific visualization symposium, pp 204–208
- Douglass EM, Jayne SR, Peacock S, Bryan FO, Maltrud ME (2012) Subtropical mode water variability in a climatologically forced model in the northwestern Pacific Ocean. *J Phys Oceanogr* 42(1):126–140
- ElNaghy H, Hamad S, Khalifa ME (2013) Taxonomy for 3D content-based object retrieval methods. *Int J Recent Res Appl Stud* 14(2):412–446
- Fujishiro I, Maeda Y, Sato H, Takeshima Y (1996) Volumetric data exploration using interval volume. *IEEE Trans Vis Comput Graph* 2(2):144–155
- Gao W, Li P, Xie SP, Xu L, Liu C (2016) Multicore structure of the North Pacific subtropical mode water from enhanced argo observations. *Geophys Res Lett* 43(3):1249–1255
- Han X, Li Z, Huang H, Kalogerakis E, Yu Y (2017) High-resolution shape completion using deep neural networks for global structure and local geometry inference. In: Proceedings of the IEEE international conference on computer vision, pp 85–93
- Hazarika S, Biswas A, Dutta S, Shen HW (2018) Information guided exploration of scalar values and isocontours in ensemble datasets. *Entropy* 20(7):540–558
- Hazarika S, Dutta S, Shen HW (2016) Visualizing the variations of ensemble of isosurfaces. In: IEEE Pacific visualization symposium, pp 209–213
- Huber DF, Hebert M (2003) Fully automatic registration of multiple 3D data sets. *Image Vis Comput* 21(7):637–650

- Johansson J, Ljung P, Jern M, Cooper M (2006) Revealing structure in visualizations of dense 2D and 3D parallel coordinates. *Inf Vis* 5(2):125–136
- Lian Z, Godil A, Sun X (2010) Visual similarity based 3D shape retrieval using bag-of-features. In: 2010 Shape modeling international conference, pp 25–36
- Lindstrom P, Turk G (2000) Image-driven simplification. *ACM Trans Graph* 19(3):204–241
- Lin J, She MF, Tsai MH, Lin IC, Lau YC, Liu HH (2018) Retrieving 3D objects with articulated limbs by depth image input. In: *VISIGRAPP (1: GRAPP)*, pp 101–111
- Liu L, Silver D, Bemis K, Kang D, Curchitser E (2017) Illustrative visualization of mesoscale ocean eddies. *Comput Graph Forum* 36(3):447–458
- Locarnini RA, Mishonov AV, Antonov JI, Boyer TP, Garcia HE, Baranova OK, Zweng MM, Paver CR, Reagan JR, Johnson DR, Hamilton M, Seidov D (2013) World ocean atlas volume 1: temperature. NOAA Atlas NESDIS 73, Silver Spring, MD 40:2013
- Masumoto Y, Sasaki H, Kagimoto T, Komori N, Ishida A, Sasai Y, Miyama T, Motoi T, Mitsudera H, Takahashi K, Sakuma H, Yamagata T (2004) A fifty-year eddy-resolving simulation of the world ocean—preliminary outcomes of OFES (OGCM for the earth simulator). *J Earth Simul* 1:35–56
- Masuzawa J (1969) Subtropical mode water. In: *Deep sea research and oceanographic abstracts*, vol 16, no 5. Elsevier, Amsterdam, pp 463–468
- Nishikawa S, Tsujino H, Sakamoto K, Nakano H (2010) Effects of mesoscale eddies on subduction and distribution of subtropical mode water in an eddy-resolving OGCM of the western North Pacific. *J Phys Oceanogr* 40(8):1748–1765
- Ohbuchi R, Osada K, Furuya T, Banno T (2008) Salient local visual features for shape-based 3D model retrieval. In: *Shape modeling and applications*, pp 93–102
- Oka E, Qiu B, Takatani Y, Enyo K, Sasano D, Kosugi N, Ishii M, Nakano T, Suga T (2015) Decadal variability of subtropical mode water subduction and its impact on biogeochemistry. *J Oceanogr* 71(4):389–400
- Qi CR, Su H, Nießner M, Dai A, Yan M, Guibas LJ (2016) Volumetric and multi-view cnns for object classification on 3d data. In: *Proceedings of the IEEE conference on computer vision and pattern recognition*, pp 5648–5656
- Shih JL, Chen HY (2006) 3D model retrieval based on grid sphere and dodecahedral silhouette descriptors. In: 9th joint international conference on information sciences (JCIS-06), Atlantis Press
- Shilane P, Min P, Kazhdan M, Funkhouser T (2004) The princeton shape benchmark. In: *Shape modeling applications*, pp 167–178
- Su H, Maji S, Kalogerakis E, Learned-Miller E (2015) Multi-view convolutional neural networks for 3d shape recognition. In: *Proceedings of the IEEE international conference on computer vision*, pp 945–953
- Talley LD (1999) Some aspects of ocean heat transport by the shallow, intermediate and deep overturning circulations. In: Clark U, Webb S, Keigwin D (eds) *Mechanisms of global climate change at millennial time scales*. Geophysical monograph series, vol 112. AGU, Washington, D.C., pp 1–22
- Tao J, Imre M, Wang C, Chawla NV, Guo H, Sever G, Kim SH (2018) Exploring time-varying multivariate volume data using matrix of isosurface similarity maps. *IEEE Trans Vis Comput Graph* 25(1):1236–1245
- Tenth Report of the Joint Panel on Oceanographic Tables and Standards. UNESCO Technical Papers in Marine Science, vol 36 (1981)
- Toyama K, Suga T (2011) Roles of mode waters in the formation and maintenance of central water in the North Pacific. In: *New developments in mode-water research*. Springer, Tokyo, pp 75–88
- Usui N, Wakamatsu T, Tanaka Y, Hirose N, Toyoda T, Nishikawa S, Fujii Y, Takatsuki Y, Igarashi H, Nishikawa H, Ishikawa Y, Kuragano T, Kamachi M (2017) Four-dimensional variational ocean reanalysis: a 30-year high-resolution dataset in the western North Pacific (FORA-WNP30). *J Oceanogr* 73(2):205–233
- Vranic DV, Saupe D (2004) 3D model retrieval. Doctoral Dissertation, University of Leipzig, pp 1–227
- Wei TH, Chen CM, Woodring J, Zhang H, Shen HW (2017) Efficient distribution-based feature search in multi-field datasets. In: *IEEE Pacific visualization symposium*, pp 121–130
- Weissenböck J, Fröhler B, Gröller E, Kastner J, Heinzl C (2018) Dynamic volume lines: visual comparison of 3D volumes through space-filling curves. *IEEE Trans Vis Comput Graph* 25(1):1040–1049
- Xie Z, Xu K, Shan W, Liu L, Xiong Y, Huang H (2015) Projective feature learning for 3D shapes with multi-view depth images. *Comput Graph Forum* 34(7):1–11
- Xu L, Xie SP, McClean JL, Liu Q, Sasaki H (2014) Mesoscale eddy effects on the subduction of North Pacific mode waters. *J Geophys Res: Oceans* 119(8):4867–4886
- Xu L, Xie SP, Liu Q, Liu C, Li P, Lin X (2017) Evolution of the North Pacific subtropical mode water in anticyclonic eddies. *J Geophys Res: Oceans* 122(12):10118–10130
- Yano M, Itoh T, Tanaka Y, Matsuoka D, Araki F (2018) Comparative 3D visualization tool for observation of mode water. In: *IEEE Pacific visualization symposium*, pp 230–234
- Yasuda T, Kitamura Y (2003) Long-term variability of North Pacific subtropical mode water in response to spin-up of the subtropical gyre. *J Oceanogr* 59(3):279–290
- Zhou H, Yuan X, Qu H, Cui W, Chen B (2008) Visual clustering in parallel coordinates. *Comput Graph Forum* 27(3):1047–1054
- Zweng MM, Reagan JR, Antonov JI, Locarnini RA, Mishonov AV, Boyer TP, Garcia HE, Baranova OK, Johnson DR, Seidov D, Biddle MM (2013) World ocean atlas volume 2: salinity. NOAA Atlas NESDIS 74. Silver Spring, MD 39:2013